Probing the electronic properties of gap states near the surface of n-SrTiO$_{3-\delta}$/i-Si(001) heterojunctions with high sensitivity

S. A. Chambers,[1] Z. H. Lim,[2,*] J. H. Ngai,[2] D. Biswas,[3] and T.-L. Lee [3]

[1]*Physical Sciences Division, Physical & Computational Sciences Directorate, Pacific Northwest National Laboratory, Richland, Washington 99352, USA*

[2]*Department of Physics, University of Texas-Arlington, Arlington, Texas 76019, USA*

[3]*Diamond Light Source, Ltd., Harwell Science and Innovation Campus, Didcot, Oxfordshire OX11 0DE, England, United Kingdom*

We have measured soft x-ray resonant photoemission for the n-SrTiO$_{3-\delta}$/i-Si(001) ($\delta = \sim 0.0003$) hybrid semiconductor heterojunction with the goal of probing occupied electronic states in the band gap near the surface. By utilizing both swept energy, angle-integrated and fixed-energy, and angle-resolved spectroscopies, we identify the atomic and orbital character of the in-gap state as well as the different electronic phases that contribute to it. Specifically, we isolate the state associated with trapped charge on the n-SrTiO$_{3-\delta}$ surface that causes surface depletion from the localized gap state resulting from electron correlation effects in the complex oxide. Using an x-ray energy close to select dipole allowed Ti $L_3 \rightarrow 3d$ x-ray absorption resonances results in a 40-fold increase in sensitivity. This feature makes photoemission possible when probing electrons from dopants at concentrations as low as a few hundredths of a percent.

I. INTRODUCTION

Semiconducting heterojunctions that exhibit built-in electric fields are the building blocks for virtually all electronic device technologies, ranging from transistors and semiconducting lasers to solar cells. While heterojunctions have traditionally been comprised of covalently bonded semiconductors, recent interest has focused on hybrid heterojunctions in which charge transfer occurs between a conventional semiconductor and a complex oxide. Ionically bonded complex oxide semiconductors fundamentally differ from their covalent counterparts. While the behavior of itinerant carriers in conventional semiconductors can be largely described by semiclassical models, this approach breaks down for complex oxides. The high carrier densities, smaller bandwidths, and large carrier effective masses give rise to strong electron-electron correlation in complex oxides. The electronic structure and behavior that arise from correlation are important to probe and understand in hybrid heterojunctions.

For example, complex oxides such as n-type SrTiO$_3$ (STO) can exhibit occupied electronic states in the band gap due to on-site Coulomb repulsion of carriers in the Ti $3d$-derived conduction band (CB). This effect has been observed in ultrahigh vacuum, low-temperature cleaved STO(001) which exhibits a two-dimensional electron gas in the near-surface region, even without a bulk dopant [1]. In this case, conductivity arises presumably as a result of fractoemission of oxygen, leading to oxygen vacancy (V_O) donor doping [2]. This effect in turn results in a broad split-off band within the

band gap containing localized carriers (the in-gap or IG state), in addition to an itinerant electron band with its leading edge at the Fermi energy (the quasiparticle or QP state). The V_O donor is particularly convenient for investigating the evolution of QP and IG states as a function of donor concentration in STO because V_O is convenient to introduce and easy to control by means of soft x-ray irradiation and O$_2$ dosing. Previous investigations have shown that intense soft x-ray beams rapidly generate V_O, resulting in itinerant and localized electrons over a wide concentration range [3–6]. Moreover, these donors are readily annihilated by dosing the surface *in situ* with a beam of O$_2$ which is conveniently dissociated and thus activated by the soft x-ray beam.

Density functional theory (DFT) establishes that the IG state originates from electron correlation in STO. The reduction in symmetry resulting from V_O creation adjacent to a B-site Ti cation results in mixing of the Ti $3d_{3z^2-r^2}$ and $4p_z$ orbitals (where the Ti-V_O-Ti bond direction is oriented along the z axis) and yields a localized state ~ 1 eV lower in energy than that of the Ti $3d_{3z^2-r^2}$ orbital in the absence of V_O. This deep level is well described using a localized impurity wave function involving the hybrid Ti $3d_{3z^2-r^2}$/$4p_z$ orbital. Moreover, strong on-site Coulomb repulsion within this state means that of the two electrons originating from V_O, only one can occupy this orbital; the other electron resides at the conduction band minimum (CBM) and is itinerant [7,8]. The localized electron screens the adjacent B-site Ti cation and causes its formal charge to drop from 4+ to 3+. V_O species arise in STO within hybrid heterojunctions as successful molecular beam epitaxy (MBE) growth of STO on Si requires a low oxygen partial pressure to prevent amorphous SiO$_2$ formation at the interface.

Additionally, donors in Si provide another source of electrons for STO within hybrid heterojunctions. Epitaxial STO

---

*Present address: TSMC R&D Center, No. 8, Lixing 6th Rd, East District, Hsinchu City 300, Republic of China.

deposited on Czochralski-grown (CZ) intrinsic Si by MBE exhibits a vastly different electronic structure than that resulting from STO deposited on *n*- and *p*-Si. Residual oxygen impurities in the near-surface region of CZ-grown Si, in conjunction with oxygen that diffuses into the Si during the epitaxial growth of STO, are found to be shallow donors [9,10]. Electrons from ionized oxygen impurity donors drift across the interface to the STO, driving depletion and even inversion in the Si, as signified by the formation of a hole gas [9]. The initiating step in this process has recently been identified as electron trapping at the STO surface driven by surface depletion, with adsorbed oxygen at Ti sites in the terminal unit cell being a viable candidate for the trap site [11]. Surface depletion promotes electron transfer across the buried interface, space charge formation within the Si, and the resulting upward (downward) band bending in the Si (STO) at the interface. As more electrons cross the interface, the type-II (staggered) band alignment observed years earlier for STO on *n*- and *p*-Si [12,13] is observed to transition to a type-III (broken) band alignment as the Si valence band maximum (VBM) crosses the Fermi level and the STO CBM drops in energy at the interface [14]. This change in band alignment can be attributed to the effect that space charge has on the interfacial dipole associated with bonding across the interface.

Thus, the STO within hybrid heterojunctions provides a rich setting in which itinerant carriers coexist with localized carriers that are spatially distributed in the bulk and surface. Determining the energies and spatial distributions of these various carriers is important to elucidating the physics governing hybrid heterojunctions. It is thus of interest to probe the properties of distributed carriers in occupied states within the band gap of V_O-doped STO grown on *i*-Si. Accordingly, our goal is to deepen our understanding of the electronic properties of (1) itinerant electrons at the bottom of the Ti 3*d*-derived CB in epitaxial STO on *i*-Si(001), and (2) electrons associated with the space-charge region at the surface which is critical for driving hole gas formation at the buried interface.

Photoemission is a useful experimental probe of occupied states at or near the surface of solids. However, the V_O concentration and thus the carrier density in these STO films is of the order of parts per ten thousand. Significantly, the QP and IG states are not readily measurable by direct photoemission at this low dopant concentration [15]. A more sensitive method is needed. Here, we show that resonant photoemission [16] exhibits the sensitivity required for this measurement, provided the x-ray absorption cross section for the transition that yields the desired photoemission final state is sufficiently large. Resonant photoemission was used to measure gap states in 100-nm epitaxial films of heavily doped $SrNb_{\sim0.06}Ti_{0.94}O_3$ deposited on $LaAlO_3$(001) by pulsed laser deposition [17] and has been used to investigate free surfaces and shallow interfaces of STO in the ensuing years [18–23]. Here, we apply the technique to 12-nm $SrTiO_{3-\delta}$ ($\delta = 0.0003$) grown on *i*-Si(001) by MBE for which the equivalent dopant density in the STO is $\sim400\times$ lower than in early STO films for which resonant photoemission was utilized [17]. We photoionize using x rays of energy in the vicinity of the Ti $L_3 \rightarrow 3d\,e_g$ absorption resonances to enhance the resonant photoemission channel. In this way, the coherent two-step process $2p^6 3d^n + \hbar\omega_{\text{res}} \rightarrow 2p^5 3d^{n+1} \rightarrow 2p^6 3d^{n-1} + e^-$ yields

the same final state as the analogous, weak direct photoemission channel $2p^6 3d^n + \hbar\omega \rightarrow 2p^6 3d^{n-1} + e^-$ excited away from resonance, but with much more intensity.

II. EXPERIMENTAL AND MODELING DETAILS

Epitaxial $SrTiO_{3-\delta}$ films were grown on nominally undoped Czochralski-grown (CZ) Si substrates using oxide MBE as described in detail elsewhere [9,14]. The V_O concentration was determined from Hall measurements for analogously deposited 12-nm STO films on float-zone (FZ) Si(001) for which electron transfer from the Si to the STO, and thus hole gas formation, does not occur to any significant extent owing to the absence of sufficient O donors in FZ Si. The sheet carrier density in such STO films is $\sim3.3 \times 10^{13}\,\text{cm}^{-2}$ leading to an estimated δ value of ~0.0003.

Hard x-ray photoemission (HAXPES) and soft x-ray resonant photoemission were carried out on the *I* and *J* branches, respectively, of Beamline I09 at Diamond Light Source. All spectra were taken with a Scienta/Omicron EW4000 hemispherical analyzer. Si 2*p*, Sr 3*d*, and Ti 2*p* core levels were measured at an x-ray energy of 5.95 keV to verify that the built-in potentials that give rise to two-dimensional (2D) hole gas were present as described in detail elsewhere [9]. For both hard and soft x-ray measurements, the beam was laterally defocused and, in some cases, the undulator was detuned to significantly lower the x-ray brightness on the sample surface and minimize if not prevent V_O creation. It is noteworthy that in previous studies for which the goal was to use the incident beam to generate itinerant electrons via V_O creation, in-gap state intensities much higher than those measured here developed in a matter of minutes due to significantly higher x-ray brightness [3–6]. The absence of an IG feature at x-ray energies far from photoemission-enhancing absorption resonances [see Fig. 1(b)] is consistent with little or no itinerant electron generation by the beam. The exceedingly weak in-gap features we observe are at an intensity level consistent with the rather low V_O doping level in the films, as described above. Angle-resolved resonant photoemission spectra were taken simultaneously by binning the total intensity map from the wide-angle detector into seven sectors of width 7.1°, as shown schematically in Fig. 4.

III. RESULTS AND DISCUSSION

To illustrate the sensitivity realized by using an x-ray energy close to the appropriate resonance, we show in Fig. 1 a Ti 2*p* spectrum excited at $\hbar\omega = 930$ eV [panel (a)] and three IG spectra excited well below, close to and above key Ti $L_3 \rightarrow 3d$ absorption resonances [panel (b)]. The photoelectron kinetic energies in these four spectra are quite close in value (450–470 eV) leading to comparable probe depths of ~2.0 nm, as discussed below. Fitting the Ti 2*p* spin-orbit doublet to a pair of Voigt functions reveals that there is no detectable intensity at the binding energies expected for the Ti^{3+} features which fall ~1.2 eV to lower binding energy from the $j = 3/2$ and 1/2 peaks for Ti^{4+}. A previously published analysis of this core level shows that Ti^{3+} is detectable when it constitutes $\sim1\%$ of the total intensity [15]. We thus verify that the δ value in these films is less than 0.005, consistent
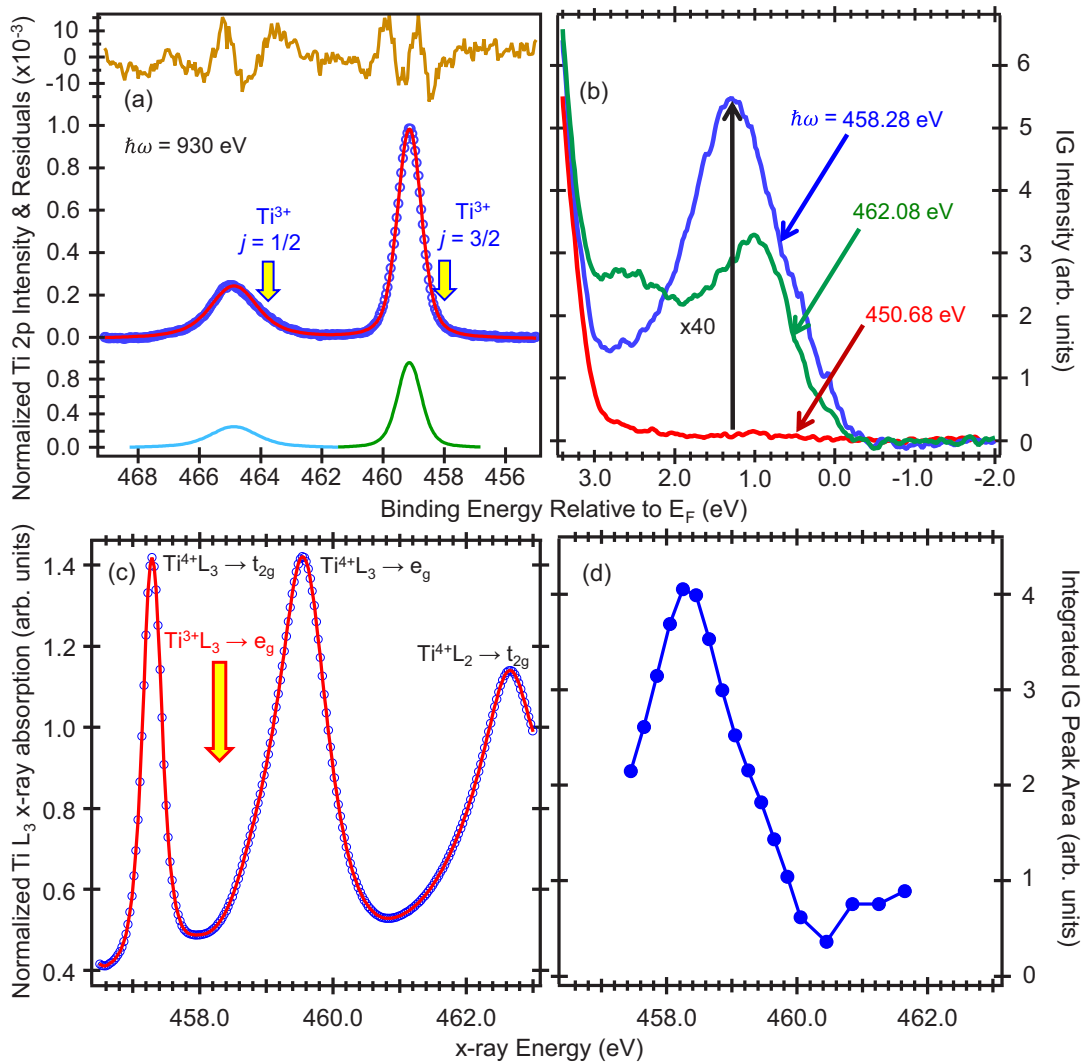
FIG. 1. Ti $2p$ core level (a) and gap-state photoemission (b) spectra for 12-nm MBE-grown SrTiO$_{2.9997}$ epitaxial films on i-Si(001). The latter were excited using x-ray energies below, near to, and above key Ti $L_3 \rightarrow 3d$ x-ray absorption resonances. The complete absence of features in the Ti $2p$ spectrum at energies corresponding to the presence of Ti^{3+} (marked by arrows) reveals that the V_O concentration is well below ~ 0.5 at. %, as explained in the text. X-ray absorption spectra (c) and IG peak area above background vs x-ray energy (d) taken from the spectra shown in Figs. 2(b).

with transport results. Sub-1% doping levels clearly pose a substantial detection challenge for conventional photoemission. However, Fig. 1(b) shows that the gap spectrum excited near the appropriate resonance exhibits excellent signal above background. We note that this maximally intense spectrum, taken at $\hbar\omega = 458.28$ eV, actually falls in the valley between the Ti^{4+} $L_3 \rightarrow 3d$ t_{2g} and Ti^{4+} $L_3 \rightarrow 3d$ e_g resonances [panel (c)] for reasons explained below. In contrast, the IG feature is barely visible at 450.68 eV, which is below these resonances. Significantly, the IG feature at $\hbar\omega = 458.28$ eV is $\sim 40\times$ more intense than that at $\hbar\omega = 450.68$ eV. Therefore, this spectroscopic approach has sufficient sensitivity to investigate gap states populated by carriers coming from sub-1% dopant concentrations.

Figure 2(a) shows the family of as-measured gap spectra excited with x-ray energies ranging 457.88–462.68 eV. This range encompasses the strong Ti $L_3 \rightarrow 3d$ x-ray absorption resonances in STO. Two prominent features are seen, one

fixed at ~ 1.5 eV binding energy and one that disperses to lower binding energy with increasing photon energy. The first of these is the IG state. The second is the Ti $2p_{3/2}$ core level (CL) generated by second-order diffracted x rays from the grating monochromator [24]. Inasmuch as this feature strongly overlaps with the QP and IG peaks as it marches across the spectrum, it must be removed to facilitate analysis of the gap spectra. To this end, we extract the Ti $2p_{3/2}$ line shape from the spectrum taken at $\hbar\omega = 462.68$ eV and use it to remove this CL from all the other spectra shown in Fig. 2(a). Figure 2(b) shows the gap spectra after removal of the Ti $2p_{3/2}$ CL. The QP feature is quite weak. However, the IG feature shows good intensity across the photon energy range. Based on *in situ* X-ray photoemission spectroscopy (XPS) results for different thicknesses of MBE-grown STO on Ge(001), we determine the photoelectron attenuation length for ~ 463 eV excitation to be 0.66 nm, leading to a probe depth of ~ 2.0 nm [25].
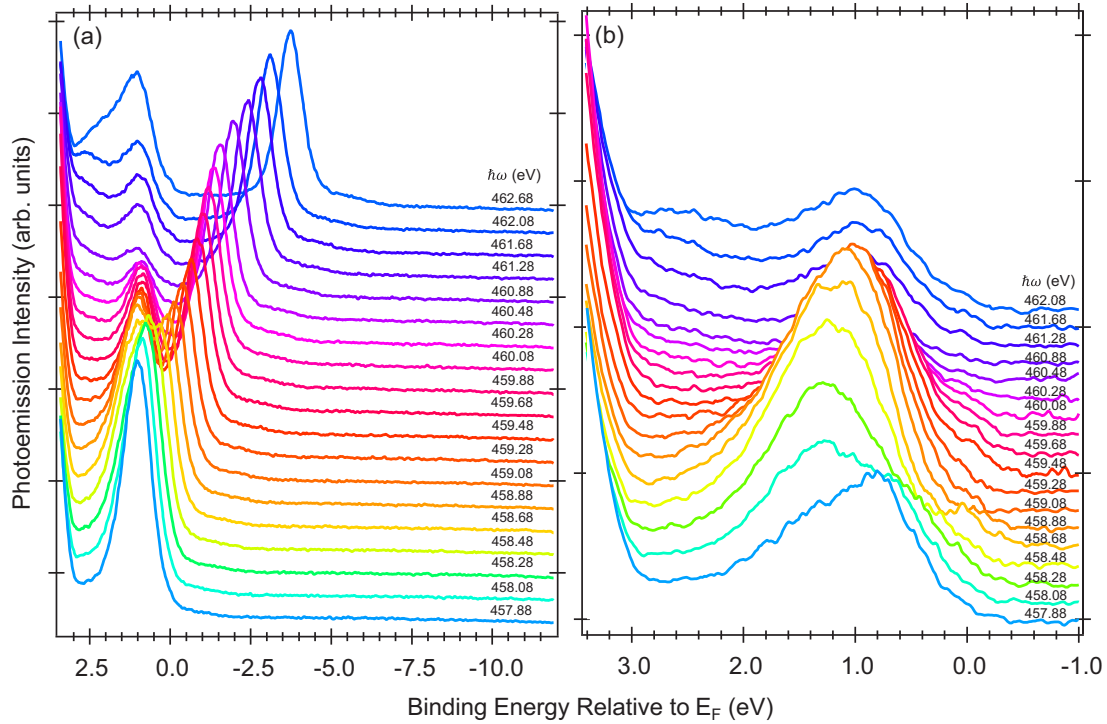
FIG. 2. Resonant photoemission spectra near the Ti $L_3 \rightarrow 3d\, e_g$ x-ray absorption resonance for 12-nm MBE-grown SrTiO$_{2.9997}$ epitaxial films on *i*-Si(001) as measured (a) and after removal of the Ti $2p_{3/2}$ spectrum excited by second-order x rays (b) which is seen to disperse with x-ray energy in panel (a).

Returning to Fig. 1, panels (c) and (d) show the x-ray absorption spectrum and the integrated IG peak areas as a function of x-ray energy, respectively. The QP feature is so weak that obtaining accurate intensities is not possible. Indeed, the inherent weakness of the QP feature is exacerbated by noise introduced when subtracting the second-order Ti $2p_{3/2}$ CL (see Fig. 2). As a result, the uncertainty in the QP peak areas is sufficiently large that a meaningful trend cannot be extracted from the data. In contrast, the much more intense IG feature clearly maximizes at ~ 458.3 eV which is quite close to the Ti^{3+} $L_3 \rightarrow 3d\, e_g$ absorption resonance for epitaxial LaTiO$_3$ [26]. Thus, the IG state is populated by electrons that are localized at *B*-site Ti cations and the close proximity of these electrons to Ti cations results in reduction from (formally) Ti^{4+} to (formally) Ti^{3+}, as expected from theory and observed for other systems [18–23].

Inspection of the band-edge profiles extracted from core-level spectra measured at $\hbar\omega = 5.95$ keV reveal upward band bending at the film surface, consistent with charge trapping at the surface leading to surface depletion [9]. Strongly adsorbed oxygen atoms at undercoordinated Ti sites on the surface have been shown to be effective electron traps that could drive this phenomenon [11]. A question that naturally arises is do these trapped electrons generate a unique feature that contributes to the gap spectrum? In order to address this question, we measured the resonant photoemission spectrum at an x-ray energy close to the Ti^{3+} $L_3 \rightarrow 3d\, e_g$ absorption resonance in angle-resolved mode to impart some level of depth resolution. Figure 3 shows gap spectra excited at $\hbar\omega = 459.30$ eV with the detector output binned into seven slices of width equal to $7.1\,°$ and central take-off angles (θ_t) ranging 39.6–82.4°. To

simplify the analysis of the IG feature, the sample normal was tilted away from the analyzer such that the QP feature was
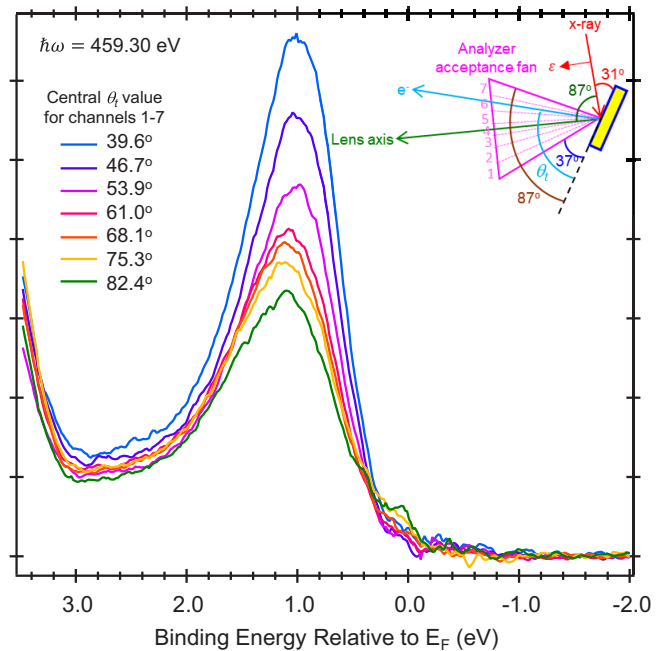

FIG. 3. In-gap spectra above the Ti^{3+} $L_3 \rightarrow 3d\, e_g$ x-ray absorption onset ($\hbar\omega = 490.30$ eV) for 12-nm MBE-grown SrTiO$_{2.9997}$ epitaxial films on *i*-Si(001) as a function of take-off angle (θ_t) relative to the plane of the surface. A schematic of the measurement is shown as an inset.
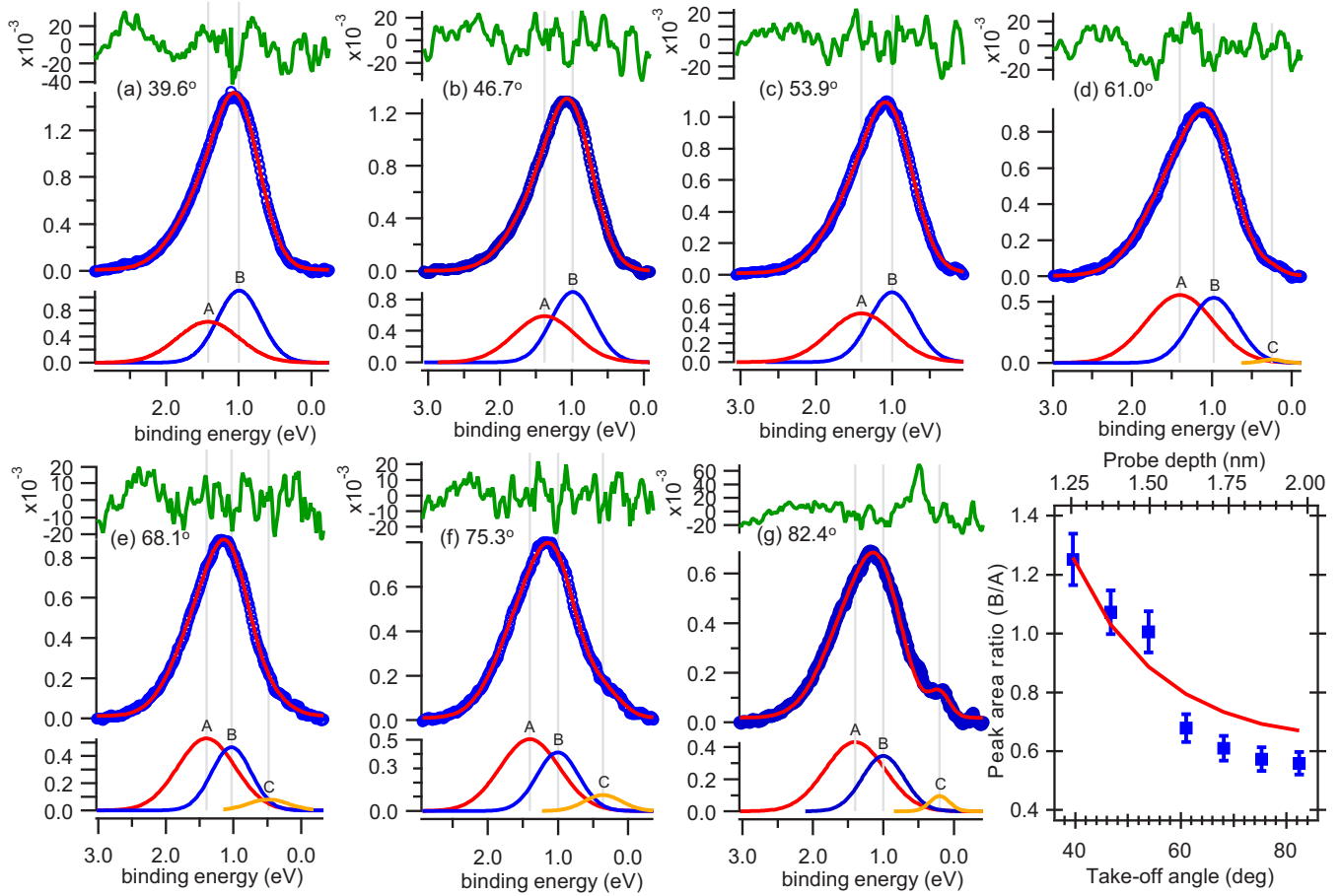
FIG. 4. Fits of the individual spectra shown in Fig. 3 to Gaussians (a)–(g). Feature *C* is the QP peak and features *A* and *B* originate from electronically distinct IG bands. Panel (h) shows the *A:B* peak area ratio as a function of take-off angle, along with a model calculation (red curve) in which it is assumed that one of the two features originates from charge trapped at the surface and the other from the localized band that runs throughout the film. Comparison of experiment and theory allows feature *B* to be assigned to the band of trapped charge at the surface.

blocked from the detector as much as possible. Additionally, the second-order Ti $2p_{3/2}$ peak in each spectrum was removed as described above, and each spectrum was normalized using the second-order Ti $2p_{3/2}$ peak area above background to eliminate the effect of detector sensitivity variations in the angular direction. Finally, the effect of varying the angle between the x-ray polarization vector and the outgoing photoelectron propagation direction (θ) on the photoemission cross section for the different detector slices was included by scaling each spectrum by the reciprocal of the differential photoemission cross section as calculated using the formula

$$\frac{d\sigma_{n,l}}{d\Omega} = \frac{\sigma_{n,l}}{4\pi}[1 + \beta P_2(\cos\theta) + (\delta + \gamma\cos^2\theta)\sin\theta\cos\varphi].$$

$$(1)$$

Here, P_2 is the second-order Legendre polynomial, ϕ is the angle between the x-ray propagation direction and the plane defined by the x-ray polarization ε and the outgoing photoelectron propagation direction (ϕ equals zero in this case), and β (δ and γ) is (are) the dipole (nondipole) parameter(s) for the interaction of the x-ray wave field with the photoemitting atom and orbital, Ti $3d$ in this case [27].

The strong IG feature is clearly asymmetric, suggesting the presence of at least two distinct electronic states therein. The QP peak is completely suppressed in the spectra at the lowest three take-off angles and becomes a minor but growing feature in the other four. Accordingly, each spectrum was fit using either two or three Gaussians depending on whether the QP peak is fully suppressed. The individual fits are shown in Figs. 4(a)–4(g). Feature *A* is dominant at higher take-off angles but is overtaken by feature *B* at lower take-off angles, implying that the electronic state giving rise to feature *B* is found at or near the surface. In contrast, feature *C*, the QP peak, becomes sufficiently intense that it must be included in the fit only at the higher take-off angles, indicating that the near-surface region contains a lower itinerant electron concentration than deeper layers, as expected in light of surface depletion.

Figure 4(h) shows the ratio of the measured IG peak areas (*B/A*) as a function of take-off angle and probe depth. Also shown is the prediction of a simple model consisting of a single unit cell (u.c.) at the STO surface sourcing photoemission intensity for one of the IG features and multiple subsurface unit cells within the probe depth collectively generating intensity for the other IG feature. Assuming a simple inelastic scattering attenuation model in which the count rate falls off

exponentially with layer depth, the intensities from these two electronic phases can be expressed as

$$I_{\text{surf u.c.}} \propto [n]_{\text{surf}} \frac{d\sigma_{Ti3d}(\theta, \varphi)}{d\Omega} \qquad (2)$$

and

$$I_{\text{subsurf u.c.}} \propto \sum_{i=2}^{n} \frac{d\sigma_{Ti3d}(\theta_i, \varphi_i)}{d\Omega} [n]_i \exp\left[-\frac{(i-1)c}{\lambda \sin(\theta_{t,i})}\right]. \quad (3)$$

Here, $[n]_{\text{surf}}$ is the trapped electron sheet density within the top u.c., $[n]_i$ is the sheet carrier density in the ith layer below the surface, c is the STO lattice parameter, λ is the electron attenuation length (0.66 nm), and the differential cross section is discussed above. We assume that $[n]_i$ is the same for all subsurface layers and that $[n]_{\text{surf}} = 0.82[n]_i$. This value was chosen to set the model and measured intensity ratios to the same value at the lowest take-off angle and is reasonable in light of Poisson-Schrodinger modeling of this heterojunction which yields good agreement between the model potential vs depth and the measured band-edge profile for $[n]_{\text{surf}} = [n]_i$ [9]. The fact that the measured B/A peak area ratio falls off with increasing take-off angle in a comparable way to that embodied in the model prediction supports the assignment of feature B to electrons trapped in the top u.c., presumably related to surface depletion. Likewise, feature A is justifiably assigned to the localized state that runs throughout the film. We thus conclude that the trapped electrons at the surface are bound by an energy of ~ 1 eV whereas those localized on B-site Ti cations throughout the film are bound slightly more strongly.

These results are important because surface depletion is routinely inferred when undesirable electronic dead layers are detected in transport data, but is not well understood, particularly for complex oxides. In the case of n-STO epitaxial films deposited on undoped STO(001) substrates, previous work suggested that 5 at. % La-doped films of various thicknesses result in dead-layer formation and a built-in potential at the film surface of magnitude ~ 0.7 eV, as measured by XPS [28]. However, band bending of this magnitude has not been measured for bulk n-STO(001) single crystal surfaces [29–33], nor is there evidence that intrinsic acceptor surface states pin the Fermi level so far below the CBM in clean STO(001) [15,34,35]. Indeed, a more recent re-examination of dead-layer formation and surface depletion based on a set of hybrid-MBE grown Dy-doped STO/undoped STO(001) samples shows that the built-in potential associated with the surface depletion field is below the detection limit of XPS [36].

This work also yields insight into the binding energy of electrons trapped on n-STO(001) film surfaces. Such binding energies cannot be determined from core-level HAXPES

measurements which yield information on the built-in potential at the surface due to the trapped charges. Thus, HAXPES and soft x-ray resonant photoemission are highly complementary. Together they yield insight into both the electric field resulting from trapped electrons at the surface, and the binding energies of these electrons.

The present results intersect with the broader topic of gap states at bulk n-STO(001) surfaces for which a number of fundamental investigations have been carried out. Of particular note is work by Guedes et $al.$ [37] in which these authors studied the dependence of the gap state electronic structure, as measured by photoemission, on temperature (up to $\sim$105 K), employing a temperature range that passed through the bulk STO structural phase transition at 105 K. It was demonstrated that the QP feature accompanying two-dimensional electron gas formation on the SrO-terminated surface and all but the deepest IG state (also observed at ambient temperature in Ref. [15]) disappear on surfaces with small miscut at $\sim$ 105 K. Vicinality was also found the influence the stability of the QP feature. The n-STO(001) surface, in either bulk crystal or thin epitaxial film form, thus constitutes a rich laboratory for investigating the interplay between composition, structure, and electronic properties in a prototypical complex oxide.

IV. SUMMARY

We show that resonant photoemission using x-ray energies close to those associated with strong x-ray absorption from appropriate core levels to the conduction band is a highly sensitive probe of occupied states in the gap. We demonstrate that itinerant and trapped electrons that originate from donors present at concentrations well below 1 at. % can be readily investigated with this technique. The in-gap feature measured for lightly V_O-doped STO/i-Si(001) is shown to originate from two distinct electronic states—one resulting from localization at Ti sites throughout the film and one associated with electrons trapped at the surface which in turn deplete the near-surface region of itinerant electrons. The binding energies of these two electronic phases are nearly the same, differing by only ~ 0.5 eV, with the surface trapped charge at the lower binding energy (~ 1.0 eV).

[1] A. F. Santander-Syro, O. Copie, T. Kondo, F. Fortuna, S. Pailhes, R. Weht, X. G. Qiu, F. Bertran, A. Nicolaou, A. Taleb-Ibrahimi, P. Le Fevre, G. Herranz, M. Bibes, N. Reyren, Y. Apertet, P. Lecoeur, A. Barthelemy, and M. J. Rozenberg, Nature (London) **469**, 189 (2011).

[2] J. T. Dickinson, L. C. Jensen, and A. Jahanlatibari, J. Vac. Sci. Technol. A **2**, 1112 (1984).

[3] W. Meevasana, P. D. C. King, R. H. He, S. K. Mo, M. Hashimoto, A. Tamai, P. Songsiriritthigul, F. Baumberger, and Z. X. Shen, Nat. Mater. **10**, 114 (2011).

[4] N. C. Plumb, M. Salluzzo, E. Razzoli, M. Månsson, M. Falub, J. Krempasky, C. E. Matt, J. Chang, M. Schulte, J. Braun, H. Ebert, J. Minár, B. Delley, K. J. Zhou, T. Schmitt, M. Shi, J. Mesot, L. Patthey, and M. Radovic, Phys. Rev. Lett. **113**, 086801 (2014).

[5] Z. Wang, S. M. Walker, A. Tamai, Y. Wang, Z. Ristic, F. Y. Bruno, A. de la Torre, S. Ricco, N. C. Plumb, M. Shi, P. Hlawenka, J. Sanchez-Barriga, A. Varykhalov, T. K. Kim, M. Hoesch, P. D. C. King, W. Meevasana, U. Diebold, J. Mesot, B. Moritz *et al.*, Nat. Mater. **15**, 835 (2016).

[6] L. Dudy, M. Sing, P. Scheiderer, J. D. Denlinger, P. Schutz, J. Gabel, M. Buchwald, C. Schlueter, T. L. Lee, and R. Claessen, Adv. Mater. **28**, 7443 (2016).

[7] C. Lin, C. Mitra, and A. A. Demkov, Phys. Rev. B **86**, 161102(R) (2012).

[8] C. W. Lin and A. A. Demkov, Phys. Rev. Lett. **111**, 217601 (2013).

[9] Z. H. Lim, N. F. Quackenbush, A. N. Penn, M. Chrysler, M. Bowden, Z. Zhu, J. M. Ablett, T.-L. Lee, J. M. LeBeau, J. C. Woicik, P. V. Sushko, S. A. Chambers, and J. H. Ngai, Phys. Rev. Lett. **123**, 026805 (2019).

[10] S. M. Sze, *Physics of Semiconductor Devices* (John Wiley and Sons, New York, Hoboken, NJ, 2007).

[11] M. Chrysler, J. Gabel, T.-L. Lee, Z. Zhu, T. C. Kaspar, M. E. Bowden, P. V. Sushko, S. A. Chambers, and J. H. Ngai, Phys. Rev. Mater. **7**, 084604 (2023).

[12] S. A. Chambers, Y. Liang, Z. Yu, R. Droopad, J. Ramdani, and K. Eisenbeiser, Appl. Phys. Lett. **77**, 1662 (2000).

[13] S. A. Chambers, Y. Liang, Z. Yu, R. Droopad, and J. Ramdani, J. Vac. Sci. Technol. A **19**, 934 (2001).

[14] M. Chrysler, J. Gabel, T. L. Lee, A. N. Penn, B. E. Matthews, D. M. Kepaptsoglou, Q. M. Ramasse, J. R. Paudel, R. K. Sah, J. D. Grassi, Z. Zhu, A. X. Gray, J. M. LeBeau, S. R. Spurgeon, S. A. Chambers, P. V. Sushko, and J. H. Ngai, Phys. Rev. Mater. **5**, 104603 (2021).

[15] S. A. Chambers, Y. Du, Z. Zhu, J. Wang, M. J. Wahila, L. F. J. Piper, A. Prakash, J. Yue, B. Jalan, S. R. Spurgeon, D. M. Kepaptsoglou, Q. M. Ramasse, and P. V. Sushko, Phys. Rev. B **97**, 245204 (2018).

[16] D. E. Eastman and W. D. Grobman, Phys. Rev. Lett. **30**, 177 (1973).

[17] Y. Ishida, R. Eguchi, M. Matsunami, K. Horiba, M. Taguchi, A. Chainani, Y. Senba, H. Ohashi, H. Ohta, and S. Shin, Phys. Rev. Lett. **100**, 056401 (2008).

[18] G. Drera, F. Banfi, F. F. Canova, P. Borghetti, L. Sangaletti, F. Bondino, E. Magnano, J. Huijben, M. Huijben, G. Rijnders, D. H. A. Blank, H. Hilgenkamp, and A. Brinkman, Appl. Phys. Lett. **98**, 052907 (2011).

[19] A. Koitzsch, J. Ocker, M. Knupfer, M. C. Dekker, K. Dorr, B. Buchner, and P. Hoffmann, Phys. Rev. B **84**, 245121 (2011).

[20] G. Berner, M. Sing, H. Fujiwara, A. Yasui, Y. Saitoh, A. Yamasaki, Y. Nishitani, A. Sekiyama, N. Pavlenko, T. Kopp, C. Richter, J. Mannhart, S. Suga, and R. Claessen, Phys. Rev. Lett. **110**, 247601 (2013).

[21] C. Cancellieri, M. L. Reinle-Schmitt, M. Kobayashi, V. N. Strocov, T. Schmitt, P. R. Willmott, S. Gariglio, and J. M. Triscone, Phys. Rev. Lett. **110**, 137601 (2013).

[22] P. Schutz, D. V. Christensen, V. Borisov, F. Pfaff, P. Scheiderer, L. Dudy, M. Zapf, J. Gabel, Y. Z. Chen, N. Pryds, V. A. Rogalev, V. N. Strocov, C. Schlueter, T. L. Lee, H. O. Jeschke, R. Valenti, M. Sing, and R. Claessen, Phys. Rev. B **96**, 161409(R) (2017).

[23] J. Gabel, M. Zapf, P. Scheiderer, P. Schutz, L. Dudy, M. Stubinger, C. Schlueter, T. L. Lee, M. Sing, and R. Claessen, Phys. Rev. B **95**, 195109 (2017).

[24] The continuous spectrum of wavelengths found in synchrotron light means that if soft x rays of wavelength λ and energy E are scattered from a grating with line spacing d and undergo first-order constructive interference at angle θ, then x rays of wavelength $\lambda/2$ (energy $2E$) will undergo *second-order* constructive interference at angle θ as well (viz. $\lambda = 2\lambda/2 = d\sin\theta$). As a result, we find the Ti $2p_{3/2}$ peak (binding energy = $\sim$460 eV) excited at $\hbar\omega = 920$ eV appearing in the same spectral region as the in-gap feature (binding energy = $\sim$1 eV) excited at $\hbar\omega = 460$ eV; both have a kinetic energy of $\sim$460 eV.

[25] S. A. Chambers and Y. Du, J. Vac. Sci. Technol. A **38**, 043409 (2020).

[26] P. Scheiderer, M. Schmitt, J. Gabel, M. Zapf, M. Stubinger, P. Schutz, L. Dudy, C. Schlueter, T. L. Lee, M. Sing, and R. Claessen, Adv. Mater. **30**, 1706708 (2018).

[27] M. B. Trzhaskovskaya, V. I. Nefedov, and V. G. Yarzhemsky, At. Data Nucl. Data Tables **77**, 97 (2001).

[28] A. Ohtomo and H. Y. Hwang, Appl. Phys. Lett. **84**, 1716 (2004).

[29] Y. Aiura, I. Hase, H. Bando, T. Yasue, T. Saitoh, and D. S. Dessau, Surf. Sci. **515**, 61 (2002).

[30] S. A. Chambers, T. Ohsawa, C. M. Wang, I. Lyubinetsky, and J. E. Jaffe, Surf. Sci. **603**, 771 (2009).

[31] C. Capan, G. Y. Sun, M. E. Bowden, and S. A. Chambers, Appl. Phys. Lett. **100**, 052106 (2012).

[32] S. A. Chambers, M. Gu, P. V. Sushko, H. Yang, C. M. Wang, and N. D. Browning, Adv. Mater. **25**, 4001 (2013).

[33] S. A. Chambers and P. V. Sushko, Phys. Rev. Mater. **3**, 125803 (2019).

[34] R. A. Powell and W. E. Spicer, Phys. Rev. B **13**, 2601 (1976).

[35] B. Reihl, J. G. Bednorz, K. A. Muller, Y. Jugnet, G. Landgren, and J. F. Morar, Phys. Rev. B **30**, 803 (1984).

[36] S. A. Chambers, D. Lee, Z. Yang, Y. Huang, W. Samarakoon, H. Zhou, P. V. Sushko, T. K. Truttmann, L. W. Wangoh, T.-L. Lee, J. Gabel, and B. Jalan., APL Mater. **10**, 070903 (2022).

[37] E. B. Guedes, S. Muff, W. H. Brito, M. Caputo, H. Li, N. C. Plumb, J. H. Dil, and M. Radovic, Adv. Sci. **8**, 2100602 (2021).